BioSystems 117 (2014) 30–39

Contents lists available at ScienceDirect

BioSystems

journal homepage: www.elsevier.com/locate/biosystems

Systems-level characterization of the kernel mechanism of the cyanobacterial circadian oscillator

Lan Ma[a,b,*], Rama Ranganathan[b]

[a] Department of Bioengineering, University of Texas at Dallas, Richardson, TX 75080, United States
[b] Green Center for Systems Biology, Department of Pharmacology, University of Texas Southwestern Medical Center, Dallas, TX 75390, United States

ARTICLE INFO

Article history:
Received 9 October 2013
Received in revised form
19 December 2013
Accepted 7 January 2014

Keywords:
Circadian clock
Mathematical model
Phase space
Relaxation oscillator

ABSTRACT

Circadian clock is an essential molecular regulatory mechanism that coordinates daily biological processes. Toward understanding the design principles of the circadian mechanism in cyanobacteria, the only prokaryotes reported to possess circadian rhythmicity, mathematical models have been used as important tools to help elucidate the complicated biochemical processes. In this study, we focus on elucidating the underlying systems properties that drive the oscillation of the cyanobacterial clockwork. We apply combined methods of time scale separation, phase space analysis, bifurcation analysis and sensitivity analysis to a model of the in vitro cyanobacterial circadian clock proposed by us recently. The original model is reduced to a three-dimensional slow subsystem by time scale separation. Phase space analysis of the reduced subsystem shows that the null-surface of the Serine-phosphorylated state (S-state) of KaiC is a bistable surface, and that the characteristic of the phase portrait indicates that the kernel mechanism of the clockwork behaves as a relaxation oscillator induced by interlinked positive and negative feedback loops. Phase space analysis together with perturbation analysis supports our previous viewpoint that the S-state of KaiC is plausibly a key component for the protein regulatory network of the cyanobacterial circadian clock.

1. Introduction

Diverse living organisms, from bacteria to humans, have developed complex molecular machinery of circadian clock to temporally coordinate internal biological processes of ~24 h cycle (Bell-Pedersen et al., 2005). Proper functioning of circadian clock is crucial to the survival and health of organisms. Cyanobacteria are the only prokaryotes possessing circadian rhythmicity known to date (Golden et al., 1997). Three clock genes, namely KaiA, KaiB and KaiC, were identified to be essential for the generation of the cyanobacterial circadian rhythm (Ishiura et al., 1998). Interestingly, self-sustained oscillatory phosphorylation of KaiC was reconstituted in vitro by mixing purified KaiA, KaiB and KaiC proteins at a proper stoichiometry, together with ATP (Nakajima et al., 2005). In this protein-only system, KaiC is the central player that serves as a dual auto-kinase and autophosphatase (Nishiwaki et al., 2000; Williams et al., 2002). It forms hexamer in solution. In addition, KaiC can be phosphorylated at two residues and the phosphorylation follows a particular cyclic order among its four phosphoforms. Specifically, the sequential change in the four KaiC phosphorylation states, unphosphorylated state → Threonine-phosphorylated state → Serine/Threonine-phosphorylated state → Serine-phosphorylated state, was observed in every cycle of circadian oscillation (Rust et al., 2007; Nishiwaki et al., 2007). The phosphorylation and dephosphorylation of KaiC are promoted by the other two Kai proteins. KaiA and KaiB together form complexes with KaiC, with KaiA catalyzing the phosphorylation of KaiC, while KaiB attenuating the activity of KaiA (Nishiwaki et al., 2000; Iwasaki et al., 2002; Kitayama et al., 2003).

Mathematical modeling based on experiments has become a powerful approach to quantitatively explore dynamics of biological processes at systems level. In attempting to explain and analyze the mechanism underlying the in vivo as well as the in vitro rhythm of KaiC, an array of theoretical models have been proposed (Rust et al., 2007; Clodong et al., 2007; Karafyllidis, 2012; Kulasiri et al., 2011; Kurosawa et al., 2006; Mehra, 2006; Mori, 2007; van Zon et al., 2007; Yoda, 2007; Brettschneider et al., 2010; Nagai et al., 2010; Qin et al., 2010; Eguchi et al., 2008; Li, 2009). Among these existing modeling work, several models of the in vitro Kai clockwork adequately account for not only the sequential progress of the KaiC phosphorylation states, but also the interactions among the KaiC phosphoforms, KaiA and KaiB (Brettschneider et al., 2010; Nagai et al., 2010; Qin et al., 2010; Li, 2009). These models mostly include detailed steps for

* Corresponding author at: Department of Bioengineering, The University of Texas at Dallas, 800 West Campbell Road, Mail Stop EC39, Richardson, TX 75080, United Sates. Tel.: +1 972 883 4752; fax: +1 972 883 4653.
E-mail address: lan.ma@utdallas.edu (L. Ma).

0303-2647/$ – see front matter © 2014 Elsevier Ireland Ltd. All rights reserved.
http://dx.doi.org/10.1016/j.biosystems.2014.01.002

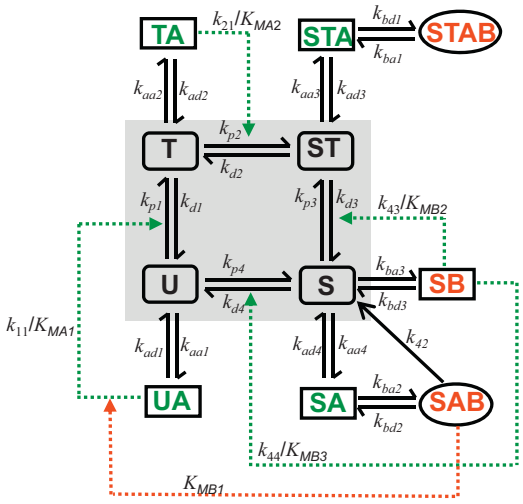

Fig. 1. Schematic diagram of our published model of cyanobacterial circadian clock. The model includes the ordered phosphorylation/dephosphorylaton among KaiC phosphoforms U, S, ST and S (plotted in shaded box), as well as the reactions among the four KaiC phosphoforms, KaiA, KaiB and their derivative complexes. In addition, UA and TA are assumed to, respectively, enhance phosphorylation from U and T, and SB is assumed to promote dephosphorylation from ST to S as well as from S to U, and SAB is assumed to inhibit the phosphorylation from U to T. Note that solid lines represent direct biochemical reactions, green dashed lines represent activating regulation, and red dashed line represent inhibitory regulation. (For interpretation of the references to color in this figure legend, the reader is referred to the web version of the article.)

KaiC hexamerization, where the coupling of the KaiC multimerization processes with the interactions among the Kai proteins renders the model considerably large-scale and intricate for further analysis. Recently, we have proposed a mathematical model of the in vitro cyanobacterial circadian clock, combining with experimental quantification, to account for the reactions of the cyclic phosphorylation/dephosphorylation of the four KaiC phosphoforms as well as the association/dissociation reactions among the various species of Kai proteins (Fig. 1) (Ma and Ranganathan, 2012). Since the KaiC protein is treated as monomer, our model is kept away from complexity of the hexamerization processes. The model is represented by 10-dimensional ordinary differential equations (ODEs), describing the dynamics of monomeric KaiC phosphoforms in free (U, T, S and ST, denoting unphosphorylated KaiC, Threonine-phosphorylated KaiC, Serine-phosphorylated KaiC and Serine/Threonine double-phosphorylated KaiC, respectively) as well as complex forms (UA, TA, SA, UAB, TAB, SAB and SB, denoting U, T, S in complex with KaiA and/or KaiB) (see Appendix A for the ODEs of the model). Computer simulations of the model have shown that it quantitatively agrees with the orderly phosphorylation of KaiC phosphoforms observed by other groups and the KaiB-C complexation kinetics measured by our FRET assay (Ma and Ranganathan, 2012).

In this paper, we ask the following questions about the clock mechanism: what underlying systems-level property drives the oscillation of the cyanobacterial clockwork? Can we dissect the dynamical network of the oscillator and further explore its embedding nonlinear feature? Can we identify plausible key component(s) of the clock mechanism? Addressing these questions will further elucidate the molecular regulatory mechanism underlying circadian clock. To this end, we apply methods of time scale separation and phase space analysis in combination with bifurcation and sensitivity analysis to our model of circadian clock. First, fast and slow timescales are separated, and the model degenerates to a slow subsystem under the classical quasi-steady state approximation of fast subsystem. Secondly, the three-dimensional slow subsystem is subjected to phase space analysis and the phase portrait demonstrates that the null-surface of the Serine-phosphorylated state (S-state) is a bistable surface, and that the trait of the phase portrait of the reduced oscillator agrees with that of a relaxation oscillator. Thirdly, bifurcation diagrams, sensitivity control coefficients together with phase space analysis indicate that the positive feedback loops are relatively more sensitive to perturbation than the negative feedback loop. And both the positive and the negative feedback loops contribute to the bistable surface in the reduced phase space. Finally, we conclude that the S state of KaiC is a key component for the protein regulatory network of the cyanobacterial circadian clock because the bistability-induced oscillation stems from the phase surface of the S state.

2. Results and discussion

2.1. Time scale separation and reduction of the model of KaiABC oscillator

To further analyze our model of circadian clock, the immediate difficulty we face is the high dimensionality of the dynamical system. By examining the model, we notice that the biochemical reactions underlying the in vitro cyanobacterial circadian oscillator undergo two different time scales: the phosphorylation and dephosphorylation of different KaiC phosphoforms progress slowly with time scale comparable to that of the circadian oscillation, while the association and dissociation among KaiA, KaiB and KaiC have relatively instantaneous reaction rates (>10-fold faster). For a multi-timescale biological system with both fast and slow reactions, the slow dynamics are typically dominating experimental observations. Thus it is eligible to apply singular perturbation theory to generate a reduced approximate slow subsystem (Khalil, 1996), which is described by a smaller number of state variables and amenable for efficient analysis and simulation. A classical example of such timescale analysis is the irreversible enzyme-catalyzed reaction, such as that of the Michaelis–Menten. For our model of cyanobacterial circadian oscillator, the interconversions among U, T, ST and S inside the shaded area depicted in the model diagram (Fig. 1) have slow rates, while the rest of the reactions in the diagram occur relatively fast. Therefore, fast state variables are identified as the seven KaiC species in complex with KaiA and KaiB, which are connected by those fast reaction rates of the model. That is, we define a fast vector x_f = [UA TA SA UAB TAB SAB SB], whose time rates of change are much larger than those of other variables. Then we can assume that these complexes of KaiC quickly settle at quasi-steady states, due to their instantaneous kinetics relative to the slow circadian dynamic with 24 h periodicity. Based on the modified singular perturbation theory and the subsequent quasi-steady state approximation (see Appendix A for theoretical basis), the original model can be reduced to a slow subsystem consisting of only three slow variables (i.e. any three species of U, T, ST and S due to conservation of the KaiC concentration) that resides on the time-varying pseudo-equilibrium point of the fast subsystem. Because previous work has indicated plausible importance of the S-state of KaiC for the circadian clock (Ma and Ranganathan, 2012), we decide to include S instead of ST in the slow subsystem and subsequent analysis.

To derive the three-dimensional subsystem mathematically, first we solve for the quasi-steady state of x_f by setting the time derivatives d[UA]/dt, d[TA]/dt, d[SA]/dt, d[UAB]/dt, d[TAB]/dt, d[SAB]/dt and d[SB]/dt to zero. In addition, we assume that the fourth order Hill functions $\frac{[B]^4}{K_{Bi}^4+[B]^4}$ (i = 1–4) equals to one because [B], the concentration of free KaiB, is much larger than K_{Bi}, the threshold constant for KaiB association. Then we analytically solve

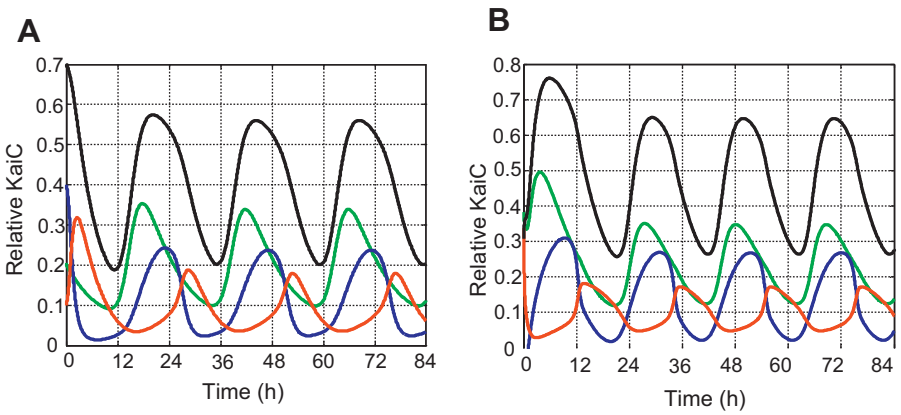

Fig. 2. Simulations of the original system (A) and the reduced system (B). Time courses of the phosphoforms T, ST, S and total phosphorylated KaiC relative to total KaiC are represented by green, blue, red and black curves, respectively. (For interpretation of the references to color in this figure legend, the reader is referred to the web version of the article.)

the following set of algebraic equations (1) for the quasi-steady state of the fast subsystem:

$$\begin{aligned}
&k_{aa1}[\mathrm{A}]\cdot[\mathrm{U}]-k_{ad1}[\mathrm{UA}]=0\\
&k_{aa2}[\mathrm{A}]\cdot[\mathrm{T}]-k_{ad2}[\mathrm{TA}]=0\\
&k_{aa3}[\mathrm{A}]\cdot[\mathrm{ST}]-k_{ad3}[\mathrm{STA}]-k_{ba1}[\mathrm{STA}]+k_{bd1}[\mathrm{STAB}]=0\\
&k_{aa4}[\mathrm{A}]\cdot[\mathrm{S}]-k_{ad4}[\mathrm{SA}]-k_{ba3}[\mathrm{SA}]+k_{bd3}[\mathrm{SAB}]=0\\
&k_{ba1}[\mathrm{STA}]-k_{bd1}[\mathrm{STAB}]=0\\
&k_{ba2}[\mathrm{SA}]-k_{bd2}[\mathrm{SAB}]-k_{42}[\mathrm{SAB}]=0\\
&k_{ba3}[\mathrm{S}]-k_{bd3}[\mathrm{SB}]=0
\end{aligned}\tag{1}$$

The quasi-steady-state concentrations of the KaiC complexes are obtained as:

$$[\mathrm{UA}]=\alpha_{\mathrm{U}}[\mathrm{A}][\mathrm{U}],\quad [\mathrm{TA}]=\alpha_{\mathrm{T}}[\mathrm{A}][\mathrm{T}],\quad [\mathrm{STA}]=\alpha_{\mathrm{ST}}[\mathrm{A}][\mathrm{ST}],$$
$$[\mathrm{STAB}]=\alpha_{\mathrm{ST}}\beta_{\mathrm{ST}}[\mathrm{A}][\mathrm{S}],\quad [\mathrm{SA}]=\alpha_{\mathrm{S}}[\mathrm{A}][\mathrm{S}],$$
$$[\mathrm{SAB}]=\alpha_{\mathrm{S}}\beta_{\mathrm{S}}[\mathrm{A}][\mathrm{S}],\quad [\mathrm{SB}]=\gamma_{\mathrm{S}}[\mathrm{S}]$$

where

$$\alpha_{\mathrm{U}}=\frac{k_{aa1}}{k_{ad1}},\quad \alpha_{\mathrm{T}}=\frac{k_{aa2}}{k_{ad2}},\quad \alpha_{\mathrm{ST}}=\frac{k_{aa4}}{k_{ad4}},\quad \beta_{\mathrm{ST}}=\frac{k_{ba1}}{k_{bd1}},$$
$$\alpha_{\mathrm{S}}=\frac{k_{aa3}}{k_{ad3}+k_{ba2}-k_{ba2}k_{ba2}/(k_{bd2}+k_{42})},\quad \beta_{\mathrm{S}}=\frac{k_{ba2}}{k_{bd2}+k_{42}},$$
$$\gamma_{\mathrm{S}}=\frac{k_{ba3}}{k_{bd3}}$$

and

$$[\mathrm{ST}]=\frac{\mathrm{KaiC}^{\mathrm{T}}-[\mathrm{U}]-[\mathrm{T}]-[\mathrm{S}]-[\mathrm{UA}]-[\mathrm{TA}]-[\mathrm{SA}]-[\mathrm{SAB}]-[\mathrm{SB}]}{1+\alpha_{\mathrm{ST}}[\mathrm{A}]+\alpha_{\mathrm{ST}}\beta_{\mathrm{ST}}[\mathrm{A}]}.$$

We see that the pseudo-equilibrium point of the fast subsystem depends on the slow variables and thus are time-varying. By substituting these pseudo-steady-state concentrations back into the slow subsystem $d[\mathrm{U}]/dt$, $d[\mathrm{T}]/dt$, $d[\mathrm{S}]/dt$, we then arrive at the final three-dimensional differential equations of the simplified system:

$$\begin{aligned}
\frac{d[\mathrm{U}]}{dt}&=-k_{p1}[\mathrm{U}]+k_{d1}[\mathrm{T}]-k_{p4}[\mathrm{U}]+k_{d4}[\mathrm{S}]-k_{aa1}[\mathrm{A}]\cdot[\mathrm{U}]+k_{ad1}[\mathrm{UA}]-k_{11}[\mathrm{U}]\frac{[\mathrm{UA}]}{K_{MA1}+[\mathrm{UA}]}\cdot\frac{1}{1+([\mathrm{SAB}]/K_{MB1})^4}+k_{12}[\mathrm{UAB}]+k_{34}[\mathrm{S}]\frac{[\mathrm{SB}]^4}{K_{MB3}^4+[\mathrm{SB}]^4}\\
\frac{d[\mathrm{T}]}{dt}&=k_{p1}[\mathrm{U}]-k_{d1}[\mathrm{T}]-k_{p2}[\mathrm{T}]+k_{d2}[\mathrm{ST}]-k_{aa2}[\mathrm{A}]\cdot[\mathrm{T}]+k_{ad2}[\mathrm{TA}]-k_{21}[\mathrm{T}]\frac{[\mathrm{TA}]}{K_{MA2}+[\mathrm{TA}]}+k_{22}[\mathrm{TAB}]+k_{11}[\mathrm{U}]\frac{[\mathrm{UA}]}{K_{MA1}+[\mathrm{UA}]}\cdot\frac{1}{1+([\mathrm{SAB}]/K_{MB1})^4}\\
\frac{d[\mathrm{S}]}{dt}&=k_{d3}[\mathrm{ST}]-k_{p3}[\mathrm{S}]+k_{p4}[\mathrm{U}]-k_{d4}[\mathrm{S}]+k_{31}[\mathrm{SAB}]-k_{aa4}[\mathrm{A}][\mathrm{S}]+k_{ad4}[\mathrm{SA}]+k_{43}[\mathrm{ST}]\frac{[\mathrm{SB}]^4}{K_{MB2}^4+[\mathrm{SB}]^4}-k_{ba3}[\mathrm{S}]\frac{[\mathrm{B}]^4}{K_{MB4}^4+[\mathrm{B}]^4}+k_{bd3}[\mathrm{SB}]-k_{44}[\mathrm{S}]\frac{[\mathrm{SB}]^4}{K_{MB3}^4+[\mathrm{SB}]^4}
\end{aligned}\tag{2}$$

Simulations show that the reduced clock system oscillates well, although with slightly elevated phosphorylated KaiC as well as smaller periodicity (~22.5 h) comparing to the original system (Fig. 2).

2.2. The simplified system is a relaxation oscillator

Plotting phase portrait with nullclines and trajectories in a two-dimensional (2D) phase plane is a standard method in dynamical systems theory to analyze and gain intuitive understanding of property of a 2D nonlinear system. Now with the simplified 3D clock system, analogously, we can plot its null-surfaces, instead of nullclines, in 3D phase space, to visualize and analyze the core mechanism of the cyanobacterial circadian rhythm. In order to obtain the null-surfaces, we set the right-hand side of $d[\mathrm{U}]/dt$, $d[\mathrm{T}]/dt$ and $d[\mathrm{S}]/dt$ in Eqs. (2) to zero, and solve for the solutions of the U-, T-, S-null-surfaces numerically using MATLAB. The null-surfaces of U, T, S thus obtained are, respectively, denoted as P1, P2 and P3 surfaces. As shown in Fig. 3A, we notice that the P1 and P2 surfaces are almost flat while the P3 surface looks significantly nonlinear. To gain a better view of the P3 surface, we remove the P2 surface, which is nearly orthogonal to the U–T plane. By choosing an appropriate visual angle, we are able to see the side profiles of the P3 and P1 surfaces (Fig. 3B and C). Intriguingly, we find that the side profile of the P3 surface projected to the P2 plane presents a rotated N-shaped feature, and the linear P1 surface intersects with the P3 surface at the intermediate portion of the N shape projected onto the P2 plane (Fig. 3C). It is well known that the hallmark of a typical 2D relaxation oscillator in its phase portrait is that a linear nullcline (or the linear part of a nullcline) intersects with the middle unstable branch of an N-shaped nullcline, where the N-shaped nullcline implicates bistability embedded in the system (Strogatz, 2001). In addition, the intersection point between the two nullclines for a 2D relaxation oscillator corresponds to an unstable equilibrium point associated with a stable limit cycle. For example, the famous nonlinear oscillator called “Van der Pol oscillator” has a straight-line nullcline intersecting with the other N-shaped nullcline at the middle branch (Strogatz, 2001). We find that the phase space portrait of our reduced system shown in Fig. 3 agrees well with these characteristics of a relaxation oscillator.

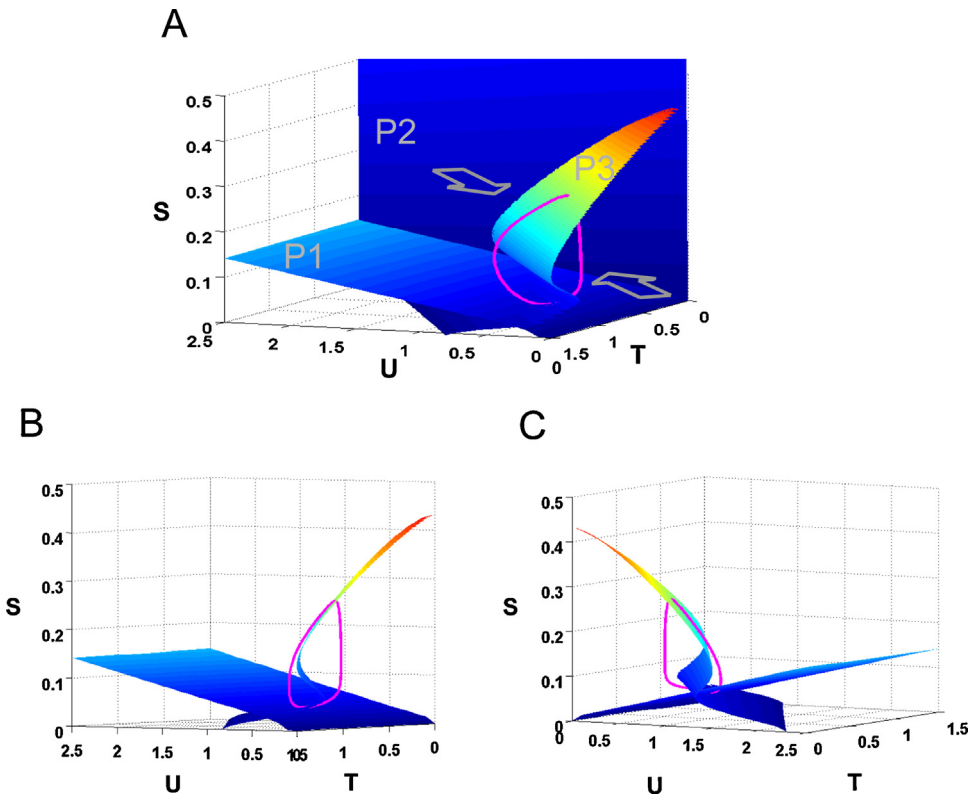

Fig. 3. Null-surfaces of the reduced system. (A) Surfaces P1, P2 and P3, corresponding to the null-surfaces of variables U, T and S, are plotted in three-dimensional phase space. P1 and P3 are re-plotted in (B) and (C) from the viewing angles listed in (A). The magenta curve represents the trajectory of the reduced system. (For interpretation of the references to color in this figure legend, the reader is referred to the web version of the article.)

With regard to time trajectories of components of a relaxation oscillator, we would expect certain asymmetry during a cycle of oscillation, in that the proportion of time spent in low state is much longer than that spent in high state. It has also been illustrated that such strong asymmetry in amplitude for a relaxation oscillator may be most evident in the trajectory of the species whose nullcline/null-surface has the rotated N-shape, as seen in the well-known FitzHugh–Nagumo relaxation oscillator (Keener, 1998) as well as other biological relaxation oscillators (Ferrell et al., 2011). Indeed the trajectory of the S-state of KaiC, who has an N-shaped null-surface, presents the highest degree of asymmetry during a cycle of oscillation (Fig. 2). Note that the total phosphorylated KaiC is the sum of three individual components (T, ST and S states of KaiC), and thus the asymmetry of a relaxation oscillator is concealed in the trajectory of the total phosphorylated KaiC.

2.3. Perturbation of the oscillator

For a 2D relaxation oscillator, the oscillation is destroyed if the fixed point shifts outside of the middle (unstable) branch of the N-shaped nullcline. A widely-known example is the "excitation block" phenomenon explained by the FitzHugh–Nagumo model, where oscillation persists only if the fixed point stays inside the middle branch of the N-shaped nullcline (Keener, 1998). To see if our model presents such type of behavior, we first perform bifurcation and sensitivity analyses of the full system to understand its behavior under perturbations. In bifurcation analysis, a single parameter value is perturbed and the steady-state response of the system is plotted at the perturbed parameter value. Such bifurcation plots are shown for parameters k_{11}, k_{p2}, k_{42}, k_{43}, k_{aa4}, k_{ba2} and k_{ba3} (Fig. 4B–H), where k_{11} and k_{p2} are rate constants regulating a long negative feedback loop, while k_{42}, k_{43}, k_{aa4}, k_{ba2} and k_{ba3} are rate constants regulating two positive feedback loops (Fig. 4A and Table 1). To quantify the degree of robustness, we define a robustness index (RI) as the minimal percentage of parameter change without abolishing the oscillations as described previously (Jacobsen and Cedersund, 2008). Specifically, the RI of a parameter is defined as: $RI \triangleq \min\left\{\frac{k_i^* - k_i^{LB}}{k_i^*}, \frac{k_i^{UB} - k_i^*}{k_i^*}\right\} = \min\left\{1 - \frac{k_i^{LB}}{k_i^*}, \frac{k_i^{UB}}{k_i^*} - 1\right\}$, where k_i^* is the nominal parameter value, k_i^{LB} and k_i^{UB} are the lower bound and upper bound of the parametric oscillation region, respectively. Intuitively, the parameter under investigation can be changed at least by the amount of RI (in percentage) without losing the oscillatory behavior. That is, the larger the value of RI of a parameter is, the more robust the system behaves with respect to that parameter. The list of oscillatory regions as well as the RIs thus calculated is given in Table 2. Interestingly, we found that the two parameters associated with the long negative feedback loop, namely k_{11} and k_{p2}, have larger values of RI than the other parameters that are associated with the positive feedback loops. Therefore, single-parameter bifurcation analysis indicates that the negative feedback loop of the circadian oscillator seems to perform more robustly than the positive feedback loops. Since oftentimes parameters associated with reverse reactions are regulated interdependently rather than independently, it is also necessary to understand robust behavior with respect to the ratio between parameters of reverse reactions. To this end, we have studied the robust behavior with respect to the ratio between k_{p2} and k_{d2} (denoted as r_1), the ratio between k_{ba3} and k_{bd3} (denoted as r_2), the ratio between k_{aa4} and k_{ad4} (denoted as r_3), as well as the ratio between k_{ba2} and k_{bd2} (denoted as r_4). That is, the ratio r_1 is associated with the negative feedback loop, while the ratios r_2, r_3 and r_4 are associated with the positive feedback loops of the circadian model. To understand the corresponding robust behavior, we need to take into account of the two degree of freedom in analyzing the sensitivity with respect to the ratios of parameters,

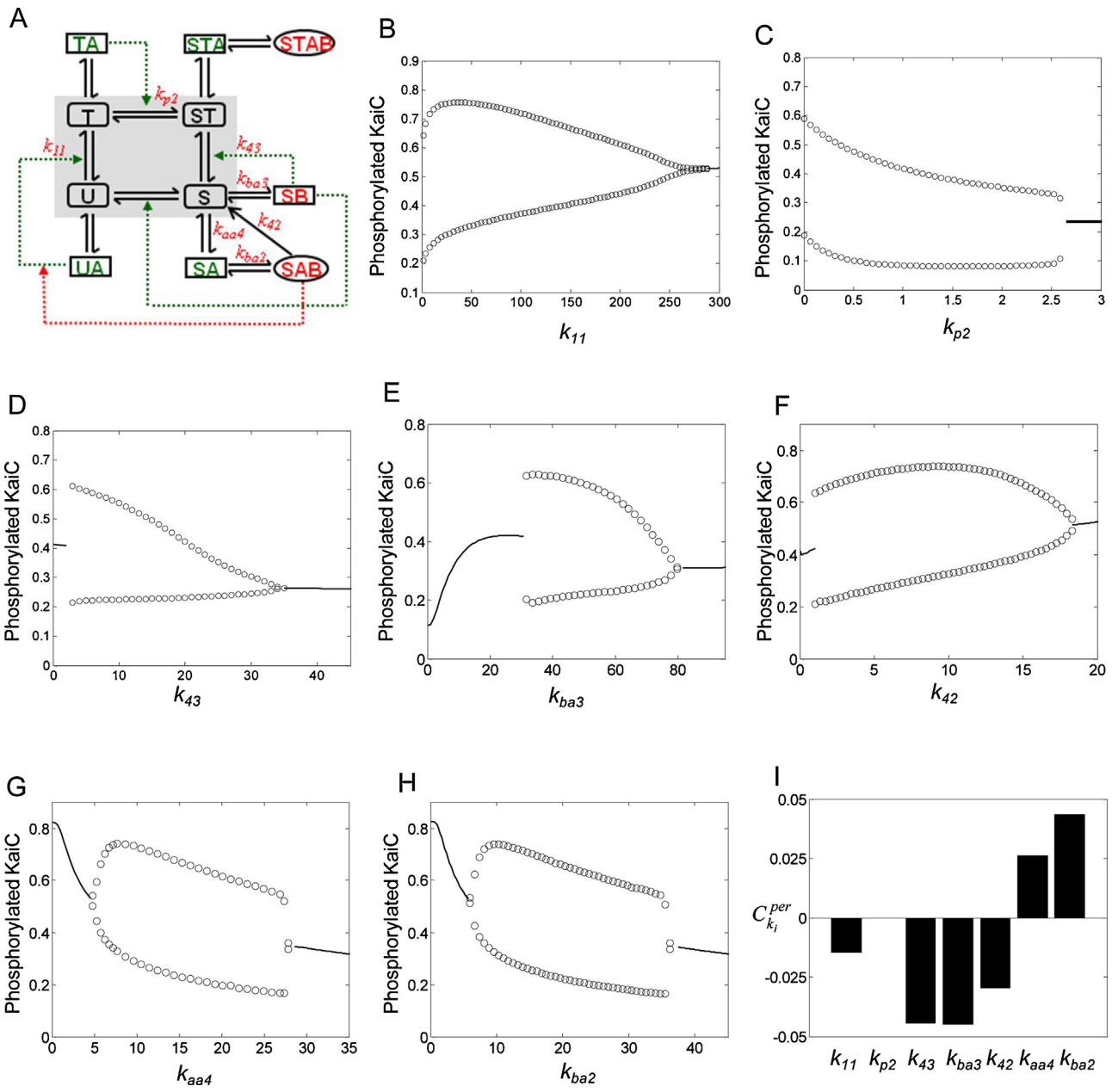

Fig. 4. Single-parameter bifurcation diagrams of the original system. Steady-state behavior of the model is plotted versus each of the parameters selected from positive and negative feedback loops as shown in (A). In (B)–(H), oscillation is represented by a pair of circles, while equilibrium point is represented by solid line. In (I), the period control coefficient $C_{k_i}^{per}$ of individual parameters are plotted. Note that $C_{k_{p2}}^{per} = 2.8 \times 10^{-4}$, and thus does not show up in the plot due to its small value. (For interpretation of the references to color in this figure legend, the reader is referred to the web version of the article.)

in that the change of values of both the numerator and the denominator would lead to change of the ratio. To this end, a bifurcation diagram at the respective nominal ratio value r_i^* is generated with respect to the numerator first. The value of r_i is then decreased or increased from r_i^* until a qualitative change in the bifurcation diagram with respect to the numerator occurs (in particular, oscillation changes to fixed point). The lower bound and upper bound at which the qualitative change occurs is denoted as r_i^{LB} and r_i^{UB}, respectively. The single-parameter bifurcation diagrams plotted at the value of r_i^*, r_i^{LB} and r_i^{UB} for all the four ratios are given in Fig. S1. Note that oscillation persists even when r_1 is increased to a significantly large value of 10^{15} $r_1^* = 3 \times 10^{14}$, therefore we assume $r_1^{UB} = \infty$. The robustness index of a ratio r_i is calculated using the same formula as that of an individual parameter: $RI(r_i) \triangleq \min\left\{1 - \frac{r_i^{LB}}{r_i^*}, \frac{r_i^{UB}}{r_i^*} - 1\right\}$.

The resulting robustness indexes are: $RI(r_1) = 0.9995$, $RI(r_2) = 0.12$, $RI(r_3) = 0.79$, and $RI(r_4) = 0.75$. Again, this analysis shows that the reaction ratio associated with the negative feedback loop can sustain higher degree of perturbation than those associated with the positive feedback loops.

Furthermore, to embody that proper periodicity is an important trait of circadian rhythm, we also calculate period control coefficient (Markus and Hess, 1990; Wolf et al., 2005; Fell, 1992) with respect to each of the parameters analyzed in Fig. 4. Specifically, we numerically compute the period control coefficient defined as $C_{k_i}^{per} = \frac{\Delta period/period}{\Delta k_i/k_i^*}$, where the quantity *period* is the periodicity of the nominal system at steady state, k_i^* is the nominal value of the parameter under investigation, Δk_i is the perturbation around its nominal parameter value, and $\Delta period$ is the resulting change of

Table 1
Parameters for the model of KaiABC circadian clock.

Parameter	Description	Units	Constant
k_{p1}	Basal phosphorylation rate of U to T	h^{-1}	1.7×10^{-4}
k_{d1}	Basal dephosphorylation rate of T to U	h^{-1}	1.7×10^{-3}
k_{p2}	Basal phosphorylation rate of T to ST	h^{-1}	5×10^{-4}
k_{d2}	Basal dephosphorylation rate of ST to T	h^{-1}	1.7×10^{-3}
k_{p3}	Basal phosphorylation rate of S to ST	h^{-1}	1.7×10^{-3}
k_{d3}	Basal dephosphorylation rate of ST to S	h^{-1}	0.067
k_{p4}	Basal phosphorylation rate of U to S	h^{-1}	5×10^{-4}
k_{d4}	Basal dephosphorylation rate of S to U	h^{-1}	0.017
k_{aa1}	Association rate between U and KaiA	$\mu M^{-1}\ h^{-1}$	57.6
k_{ad1}	Dissociation rate of UA	$\mu M^{-1}\ h^{-1}$	19.2
k_{aa2}	Association rate between T and KaiA	$\mu M^{-1}\ h^{-1}$	28.8
k_{ad2}	Dissociation rate of TA	$\mu M^{-1}\ h^{-1}$	19.2
k_{aa3}	Association rate between ST and KaiA	$\mu M^{-1}\ h^{-1}$	19.2
k_{ad3}	Dissociation rate of STA	$\mu M^{-1}\ h^{-1}$	57.6
k_{aa4}	Association rate between S and KaiA	$\mu M^{-1}\ h^{-1}$	19.2
k_{ad4}	Dissociation rate of SA	$\mu M^{-1}\ h^{-1}$	24
k_{ba1}	Association rate between STA and KaiB	$\mu M^{-1}\ h^{-1}$	28.8
k_{bd1}	Dissociation rate of STAB	$\mu M^{-1}\ h^{-1}$	38.4
k_{ba2}	Association rate between SA and KaiB	$\mu M^{-1}\ h^{-1}$	24
k_{bd2}	Dissociation rate of SAB	$\mu M^{-1}\ h^{-1}$	24
k_{ba3}	Association rate between S and KaiB	$\mu M^{-1}\ h^{-1}$	38.4
k_{bd3}	Dissociation rate of SB	$\mu M^{-1}\ h^{-1}$	19.2
k_{11}	Phosphorylation rate of U facilitated by KaiA	h^{-1}	1.44
k_{21}	Phosphorylation rate of T facilitated by KaiA	h^{-1}	0.22
k_{42}	Dephosphorylation rate of SAB to S	h^{-1}	1.44
k_{43}	Dephosphorylation rate of ST facilitated by SB	h^{-1}	1.44
k_{44}	Dephosphorylation rate of SB to U	h^{-1}	0.86
K_{MA1}	Threshold conc. for UA-dependent phosphorylation of U	μM	0.3
K_{MA2}	Threshold conc. for TA-dependent phosphorylation of T	μM	0.1
K_{MB1}	Threshold conc. for SAB-dependent phosphorylation of U	μM	0.004
K_{MB2}	Threshold conc. for SB-dependent dephosphorylation of ST	μM	0.317
K_{MB3}	Threshold conc. for SB-dependent dephosphorylation of S	μM	0.032
K_{B1}	Threshold conc. for cooperative binding of KaiB with STA	μM	1.19
K_{B2}	Threshold conc. for cooperative binding of KaiB with SA	μM	0.94
K_{B3}	Threshold conc. for cooperative binding of KaiB with S	μM	1.06

the steady-state periodicity due to perturbation Δk_i. The parametric perturbations are chosen sufficiently small to ensure a linear $\Delta k_i - \Delta period$ relationship (Wolf et al., 2005). The values of $C_{k_i}^{per}$ are plotted in Fig. 4I. Note that a period control coefficient measures the degree of sensitivity, thus the larger the value of $C_{k_i}^{per}$, the more sensitive the period response is with respect to the parameter k_i. As shown in Fig. 4I, all the period control coefficients are small (<5%), indicating that the period response of the circadian oscillator has robust performance. In addition, the periodicity is least sensitive to the perturbations in k_{11} and k_{p2}, the parameters that are associated with the negative feedback loop, consistent with the perturbation results using the measure of RI.

Overall, our results of the system performance under perturbations show that the degree of robustness with respect to the two rates associated with the negative feedback loop (k_{11} and k_{p2}) is significantly higher than that with respect to the rates associated with the positive feedback loops (k_{42}, k_{43}, k_{aa4}, k_{ba2} and k_{ba3}). In other words, we find that the positive feedback loops in the clock oscillator is more sensitive to external parametric perturbations than the negative feedback loops.

Table 2
Oscillatory region and robustness index (RI) for parameters in Fig. 4.

Parameter	Oscillatory region	RI
k_{11}	[0, 288]	1
k_{p2}	[0, 2.59]	1
k_{43}	[0.8, 35]	0.44
k_{ba3}	[31.5, 79]	0.18
k_{42}	[1, 18]	0.31
k_{aa4}	[4.8, 27.8]	0.45
k_{ba2}	[6, 36.2]	0.5

How do the perturbations in parameters affect the reduced system in terms of the phase portrait plot? For each of the above parameters embedded in feedback loops, we choose a value just outside the oscillatory region and compare the three-dimensional null-surfaces of the perturbed (non-oscillatory) and unperturbed (oscillatory) model (Fig. 5). Denoting the shift of the null-surfaces by red arrows, Fig. 5 shows that under parameter perturbations the configuration of one or more null-surfaces changes. The shift of the P2 surface seems to have the least effect on the systems behavior because decreased k_{p2} value does not abolish the oscillation, which tilts the P2 surface while the P1 and P3 surfaces remain the same (data not shown). Of note, shift of the P3 surface is induced by five of the parameters (k_{42}, k_{43}, k_{ba2}, k_{ba3}, k_{aa4}), which are directly associated with the reactions of the S-state of KaiC in the protein signaling network (Fig. 1), indicating that the N-shaped bistability surface originates from direct regulations of the S-state. This result underscores the importance of the S-state because it is known that the N-shaped null-surface/nullcline is the kernel element of a relaxation oscillator. In addition, these perturbation plots of phase portraits confirm that the systems behavior of our oscillatory model essentially is determined by the configurations of the null-surfaces.

Nevertheless, how the configurations of the 3D null-surfaces controls the oscillation of system is still unclear. Since the oscillation of the system is relatively insensitive to the perturbation in the P2 surface, we eliminate this degree of freedom by solving the intersections of the P1 and P3 surfaces with the P2 surface. As shown in Fig. 6, the intersection between P1 and P2 is a straight line except near the origin, while the intersection between P3 and P2 is an N-shaped curve. These intersection curves on P2 surface agree with the characteristics of the nullclines of a 2D relaxation oscillator. Moreover, by examination of Fig. 6 we find that under the nominal oscillatory condition the fixed point (i.e. the intersect

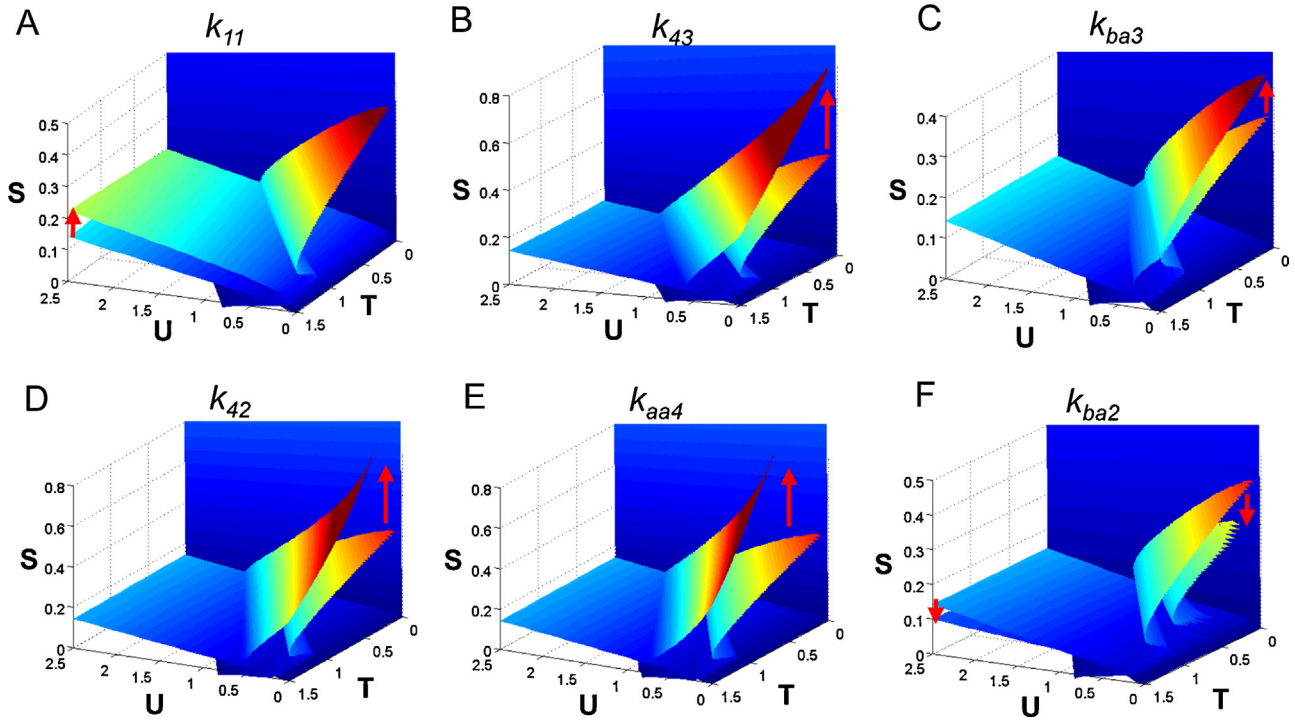

Fig. 5. Null-surfaces of the reduced system before and after perturbation of selected parameter in three-dimensional phase space. The red arrow indicates the direction of change of null-surfaces from unperturbed to perturbed situation. The perturbed parameter values are: $k_{11} = 295$, $k_{43} = 38$, $k_{ba3} = 82$, $k_{42} = 19$, $k_{aa4} = 29$, $k_{ba2} = 38$. (For interpretation of the references to color in this figure legend, the reader is referred to the web version of the article.)

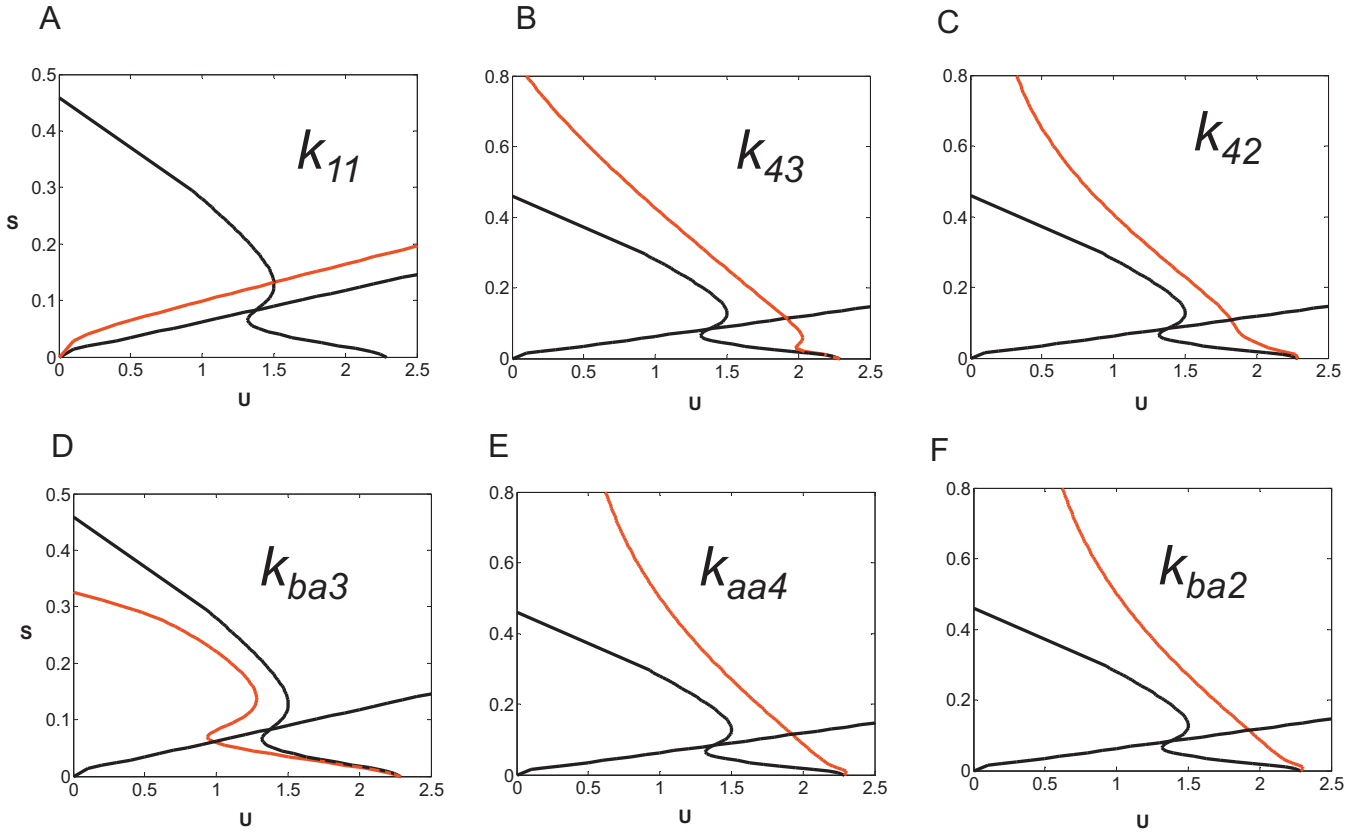

Fig. 6. Intersection lines between paired null-surfaces of the reduced system in two-dimensional phase plane. Null-surfaces P1 and P3 are projected onto P2 before (black) and after (red) the perturbation of the parameter listed in each plot. The intersection line between P1 and P2 is a straight line except near the origin, while the intersection line between P1 and P3 presents a rotated N shape. In addition, the fixed point lies in the middle branch of the N-shaped curve. After each parameter is perturbed (red), either the fixed point moves out of the middle branch of the N-shaped intersection curve, or the N-shape is lost, leading to disability of oscillation. (For interpretation of the references to color in this figure legend, the reader is referred to the web version of the article.)

point of the P1, P2 and P3 surfaces) is on the middle branch of the N-shaped curve, while the oscillation is abolished when the fixed point sits outside of the middle branch of the N-shaped curve, or when the N-shape of the bistability surface is lost. In other words, the results in Fig. 6 indicate that the fixed point of the reduced system needs to stay on the middle branch of an N-shaped nullcline to remain as an unstable fixed point, which is coupled with a limit cycle. Again, such behavior of phase portrait agrees well with that of a 2D relaxation oscillator. All together, the above phase plane analysis combined with perturbation analysis suggests that from systems perspective the kernel mechanism of our model of cyanobacterial circadian clock works as a relaxation oscillator.

3. Conclusions

In this study, we dissect a mathematical model of cyanobacterial circadian rhythm and extract its systems property. We show that the original clock model can be simplified to a three-dimensional core oscillator. In addition, phase-space portraits of the reduced oscillator combined with perturbation analysis demonstrate that the core mechanism of cyanobacterial circadian clock displays systems feature of a relaxation oscillator. For instance, the null-surfaces of the reduced system present an N-shaped bistability surface intersected with a linear surface at the middle branch of the N-shape configuration, the hallmark of a relaxation oscillator. The finding that the kernel mechanism of the cyanobacterial circadian clock behaves as a relaxation oscillator implies that the circadian rhythm of both prokaryotes and eukaryotes may share common features not only at molecular level, but also at systems level, as previous study has suggested that the underlying mechanism of eukaryotic circadian clocks also constitutes a relaxation oscillator (Tyson et al., 1999; Vilar et al., 2002). Therefore circadian clockwork in various organisms probably can be considered mechanistically converging in terms of its systems design principles. Our results also underscore the importance of the negative-plus-positive feedback network design underlying a circadian clock, which forms the essential structure of a relaxation oscillator. In particular, thepositive feedback loops mediated by the S-sate of KaiC appear crucial for maintaining the systems behavior of the KaiABC oscillator, as they are shown to be relatively less robust under external perturbations.

Notably, in the schematic diagram of the full model (Fig. 1), the S-state of KaiC is a hub element in terms of network structure, mediating two positive feedback loops ($S \rightarrow SB \rightarrow S$ and $S \rightarrow SA \rightarrow SAB \rightarrow S$) and a negative feedback loop ($S \rightarrow SA \rightarrow SAB \dashv T \rightarrow ST \rightarrow S$), which are essential for the generation of circadian oscillation (Ma and Ranganathan, 2012). The role of the S-state as a network hub indicates that the S-state of KaiC is plausibly a central component coordinating the functioning of the circadian oscillator, a viewpoint proposed previously (Ma and Ranganathan, 2012). In this work, our phase surface analysis shows that the nonlinearity associated with the null-surface of the S-state is indispensable for the core relaxation oscillator. Therefore, using systems-level analysis of the circadian model, we support, in a quantitative manner, the critical role played by the S-state of KaiC in the core mechanism of the cyanobacterial circadian clock. Further experiments will be needed to evaluate this theoretical prediction. Nevertheless, there are cyanobacterial mutant strains whose circadian rhythm is disrupted while the mechanism is not known. Based on this work, we speculate that the mechanism behind these disrupted phenotypes may probably be explained by a perturbation of the S-state of KaiC.

Acknowledgement

The authors are grateful for the Start-up Fund from the University of Texas at Dallas.

Appendix A.

The 10-dimensional ODE model of cyanobacterial circadian clock is constructed as previously published (Ma and Ranganathan, 2012) and given as follows:

$$\frac{d[U]}{dt} = -k_{p1}[U] + k_{d1}[T] - k_{p4}[U] + k_{d4}[S] - k_{aa1}[A]\cdot[U] + k_{ad1}[UA] + k_{12}[UAB] + k_{34}[S]\frac{[SB]^4}{K_{MB3}^4 + [SB]^4} - k_{11}[U]\frac{[UA]}{K_{MA1} + [UA]}\cdot\frac{1}{1 + ([SAB]/K_{MB1})^4}$$

$$\frac{d[T]}{dt} = k_{p1}[U] - k_{d1}[T] - k_{p2}[T] + k_{d2}[ST] - k_{aa2}[A]\cdot[T] + k_{ad2}[TA] - k_{21}[T]\frac{[TA]}{K_{MA2} + [TA]} + k_{22}[TAB] + k_{11}[U]\frac{[UA]}{K_{MA1} + [UA]}\cdot\frac{1}{1 + ([SAB]/K_{MB1})^4}$$

$$\frac{d[S]}{dt} = k_{d3}[ST] - k_{p3}[S] + k_{p4}[U] - k_{d4}[S] + k_{31}[SAB] - k_{aa4}[A][S] + k_{ad4}[SA] + k_{43}[ST]\frac{[SB]^4}{K_{MB2}^4 + [SB]^4} - k_{ba3}[S]\frac{[B]^4}{K_{MB4}^4 + [B]^4} + k_{bd3}[SB] - k_{44}[S]\frac{[SB]^4}{K_{MB3}^4 + [SB]^4}$$

$$\frac{d[UA]}{dt} = k_{aa1}[A]\cdot[U] - k_{ad1}[UA]$$

$$\frac{d[TA]}{dt} = k_{aa2}[A]\cdot[T] - k_{ad2}[TA]$$

$$\frac{d[STA]}{dt} = k_{aa3}[A]\cdot[ST] - k_{ad3}[STA] - k_{ba1}[STA]\frac{[B]^4}{K_{B1}^4 + [B]^4} + k_{bd1}[STAB]$$

$$\frac{d[SA]}{dt} = k_{aa4}[A]\cdot[S] - k_{ad4}[SA] - k_{ba3}[SA]\frac{[B]^4}{K_{B2}^4 + [B]^4} + k_{bd3}[SAB]$$

$$\frac{d[STAB]}{dt} = k_{ba1}[STA]\frac{[B]^4}{K_{B1}^4 + [B]^4} - k_{bd1}[STAB]$$

$$\frac{d[SAB]}{dt} = k_{ba2}[SA]\frac{[B]^4}{K_{B2}^4 + [B]^4} - k_{bd2}[SAB] - k_{42}[SAB]$$

$$\frac{d[SB]}{dt} = k_{ba3}[S]\frac{[B]^4}{K_{B3}^4 + [B]^4} - k_{bd3}[SB]$$

The eleventh KaiC species, ST, is constrained by the conservation of the total concentration of KaiC, i.e. $[U]+[T]+[ST]+[UA]+[TA]+[SA]+[UAB]+[TAB]+[SAB]+[SB]+[S] = KaiC^T$. The parameter values are listed in Table 1.

The method of model reduction we use is based on singular perturbation theory (Khalil, 1996). Suppose a dynamical system has separable fast and slow variables, denoted by x_s and x_f, respectively.

Due to the slow/fast time rate of change for slow/fast variables, the state-space representation of the model is represented as:

$$\dot{x}_s = f(t, x_s, x_f, \varepsilon), \quad x_s \in R^n \tag{3}$$

$$\varepsilon \cdot \dot{x}_f = g(t, x_s, x_f, \varepsilon), \quad x_f \in R^m \tag{4}$$

where $\varepsilon \ll 1$ is a small positive parameter, and f and g are continuously differentiable functions. On the time scale that slow variables show variation, the fast variables quickly settle to their quasi-steady-state if the fast subsystem has at least one isolated real roots. This leads to the standard singular perturbation theory that sets $\varepsilon = 0$ and the dimension of the original system reduces from $m+n$ to n because the differential equation (4) degenerates to the algebraic equation (5):

$$0 = g(t, x_s, x_f^0, 0) \tag{5}$$

Here we use a modified singular perturbation model that has improved accuracy (Gomez-Uribe et al., 2008). Using such a model, we do not set ε to 0 and the reduced slow subsystem becomes (6):

$$\dot{x}_s = f(t, x_s, h(t, x), \varepsilon) \tag{6}$$

where $h(t, x)$ is the steady-state solution for x_f^0 in the following algebraic equation (7):

$$0 = g(t, x_s, x_f^0, \varepsilon) \tag{7}$$

For our model of KaiABC oscillator, the association and dissociation rates among the Kai proteins (k_{aai} and k_{adi}, $i = 1$–4; k_{baj} and k_{bdj}, $j = 1$–3) are much bigger (~13- to 80,000-fold) than the phosphorylation and dephosphorylation rates (k_{pl} and k_{dl}, $l = 1$–4, and k_{11}, k_{21}, k_{42}, k_{43} and k_{44}). And the derivative of the fast variables x_f = [[UA] [TA] [SA] [UAB] [TAB] [SAB] [SB]] is dominated by the fast binding reactions. That is, if we rewrite $k_{aai} = (1/\varepsilon)k^*_{aai}$, $k_{adi} = (1/\varepsilon)k^*_{adi}$, $i = 1$–4, and $k_{baj} = (1/\varepsilon)k^*_{bai}$, $k_{bdj} = (1/\varepsilon)k^*_{bdi}$, $j = 1$–3, with the choice of scaling parameter $\varepsilon = 0.08$ (i.e. 1/12.5), the differential equation for the fast subsystem then takes the standard form in (4), where the vector field g is now:

$$g = \begin{bmatrix} k^*_{aa1}[\mathrm{A}]\cdot[\mathrm{U}] - k^*_{aa1}[\mathrm{UA}] \\ k^*_{aa2}[\mathrm{A}]\cdot[\mathrm{T}] - k^*_{ad2}[\mathrm{TA}] \\ k^*_{aa3}[\mathrm{A}]\cdot[\mathrm{ST}] - k^*_{ad3}[\mathrm{STA}] - k^*_{ba1}[\mathrm{STA}]\dfrac{[\mathrm{B}]^4}{K_{B1}^4 + [\mathrm{B}]^4} + k^*_{bd1}[\mathrm{STAB}] \\ k^*_{aa4}[\mathrm{A}]\cdot[\mathrm{S}] - k^*_{ad4}[\mathrm{SA}] - k^*_{ba3}[\mathrm{SA}]\dfrac{[\mathrm{B}]^4}{K_{B2}^4 + [\mathrm{B}]^4} + k^*_{bd3}[\mathrm{SAB}] \\ k^*_{ba1}[\mathrm{STA}]\dfrac{[\mathrm{B}]^4}{K_{B1}^4 + [\mathrm{B}]^4} - k^*_{bd1}[\mathrm{STAB}] \\ k^*_{ba2}[\mathrm{SA}]\dfrac{[\mathrm{B}]^4}{K_{B2}^4 + [\mathrm{B}]^4} - k^*_{bd2}[\mathrm{SAB}] - \varepsilon\cdot k_{42}[\mathrm{SAB}] \\ k^*_{ba3}[\mathrm{S}]\dfrac{[\mathrm{B}]^4}{K_{B4}^4 + [\mathrm{B}]^4} - k^*_{bd3}[\mathrm{SB}] \end{bmatrix}$$

Note that the order of derivative on the left-hand sides of Eq. (4) is not affected by the term multiplied by ε on the right-hand side because it is small and can be neglected in comparison with other right-hand-side terms. Next we examine the slow subsystem of KaiABC oscillator with the slow variable x_s = [[U] [T] [S]]. Here we have chosen to explicitly include the S-state of KaiC instead of the ST-state in the slow variables because our previous study indicates that the S phosphorylated-state of KaiC is likely a critical component in determining the dynamics of the circadian oscillator. Based on the differential equations (6), it is noteworthy that the derivative of x_s is dominated by the terms of slow phosphorylation/dephosphorylation reactions, except for one or two paired association/dissociation reactions. Since the latter are equilibrated quickly, the net rate of these reaction pairs turn out to be in the same order of magnitude as the rest of the slow terms (data not shown), and thus the resulting time rate of x_s still remains small. This appendix provides the theoretical basis for the operation of model reduction performed in the main text.

Appendix B. Supplementary data

Supplementary data associated with this article can be found, in the online version, at http://dx.doi.org/10.1016/j.biosystems.2014.01.002.

References

Bell-Pedersen, D., et al., 2005. Circadian rhythms from multiple oscillators: lessons from diverse organisms. Nat. Rev. Genet. 6 (7), 544–556.

Brettschneider, C., et al., 2010. A sequestration feedback determines dynamics and temperature entrainment of the KaiABC circadian clock. Mol. Syst. Biol. 6, 389.

Clodong, S., et al., 2007. Functioning and robustness of a bacterial circadian clock. Mol. Syst. Biol. 3, 90.

Eguchi, K., et al., 2008. Mechanism of robust circadian oscillation of KaiC phosphorylation in vitro. Biophys. J. 95 (4), 1773–1784.

Fell, D.A., 1992. Metabolic control analysis: a survey of its theoretical and experimental development. Biochem. J. 286 (Pt 2), 313–330.

Ferrell Jr., J.E., Tsai, T.Y., Yang, Q., 2011. Modeling the cell cycle: why do certain circuits oscillate? Cell 144 (6), 874–885.

Golden, S.S., et al., 1997. Cyanobacterial circadian rhythms. Annu. Rev. Plant Physiol. Plant Mol. Biol. 48, 327–354.

Gomez-Uribe, C.A., Verghese, G.C., Tzafriri, A.R., 2008. Enhanced identification and exploitation of time scales for model reduction in stochastic chemical kinetics. J. Chem. Phys. 129 (24), 244112.

Ishiura, M., et al., 1998. Expression of a gene cluster kaiABC as a circadian feedback process in cyanobacteria. Science 281 (5382), 1519–1523.

Iwasaki, H., et al., 2002. KaiA-stimulated KaiC phosphorylation in circadian timing loops in cyanobacteria. Proc. Natl. Acad. Sci. U. S. A. 99 (24), 15788–15793.

Jacobsen, E.W., Cedersund, G., 2008. Structural robustness of biochemical network models – with application to the oscillatory metabolism of activated neutrophils. IET Syst. Biol. 2 (1), 39–47.

Karafyllidis, I.G., 2012. Mechanics and resonance of the cyanobacterial circadian oscillator. Biosystems 109 (2), 137–140.

Keener, J., Sneyd, J., 1998. Mathematical Physiology, 1st ed. Springer-Verlag, New York, NY.

Khalil, H.K., 1996. Nonlinear Systems. Prentice Hall, Upper Saddle River, NJ.

Kitayama, Y., et al., 2003. KaiB functions as an attenuator of KaiC phosphorylation in the cyanobacterial circadian clock system. EMBO J. 22 (9), 2127–2134.

Kulasiri, D., He, Y., Samarasinghe, S., 2011. Robustness of circadian rhythms in the presence of molecular fluctuations: an investigation based on a mechanistic, statistical theory and a simulation algorithm. Biosystems 106 (1), 57–66.

Kurosawa, G., Aihara, K., Iwasa, Y., 2006. A model for the circadian rhythm of cyanobacteria that maintains oscillation without gene expression. Biophys. J. 91 (6), 2015–2023.

Li, C.et al., 2009. Circadian KaiC phosphorylation: a multi-layer network. PLoS Comput. Biol. 5 (11), e1000568.

Ma, L., Ranganathan, R., 2012. Quantifying the rhythm of KaiB-C interaction for in vitro cyanobacterial circadian clock. PLoS ONE 7 (8), pe42581.

Markus, M., Hess, B., 1990. Control of metabolic oscillations: unpredictability, critical slowing down, optimal stability and hysteresis. In: Cornish-Bowden, M.C.A. (Ed.), Control of Metabolic Processes. Plenum Press, New York, pp. 303–313.

Mehra, A.et al., 2006. Circadian rhythmicity by autocatalysis. PLoS Comput. Biol. 2 (7), e96.

Mori, T.et al., 2007. Elucidating the ticking of an in vitro circadian clockwork. PLoS Biol. 5 (4), e93.

Nagai, T., Terada, T.P., Sasai, M., 2010. Synchronization of circadian oscillation of phosphorylation level of KaiC in vitro. Biophys. J. 98 (11), 2469–2477.

Nakajima, M., et al., 2005. Reconstitution of circadian oscillation of cyanobacterial KaiC phosphorylation in vitro. Science 308 (5720), 414–415.

Nishiwaki, T., et al., 2000. Nucleotide binding and autophosphorylation of the clock protein KaiC as a circadian timing process of cyanobacteria. Proc. Natl. Acad. Sci. U. S. A. 97 (1), 495–499.

Nishiwaki, T., et al., 2007. A sequential program of dual phosphorylation of KaiC as a basis for circadian rhythm in cyanobacteria. EMBO J. 26 (17), 4029–4037.

Qin, X., et al., 2010. Intermolecular associations determine the dynamics of the circadian KaiABC oscillator. Proc. Natl. Acad. Sci. U. S. A. 107 (33), 14805–14810.

Rust, M.J., et al., 2007. Ordered phosphorylation governs oscillation of a three-protein circadian clock. Science 318 (5851), 809–812.

Strogatz, S., 2001. Nonlinear Dynamics and Chaos: With Applications to Physics, Biology, Chemistry and Engineering. Westview Press, Boulder, CO.

Tyson, J.J., et al., 1999. A simple model of circadian rhythms based on dimerization and proteolysis of PER and TIM. Biophys. J. 77 (5), 2411–2417.

van Zon, J.S., et al., 2007. An allosteric model of circadian KaiC phosphorylation. Proc. Natl. Acad. Sci. U. S. A. 104 (18), 7420–7425.

Vilar, J.M., et al., 2002. Mechanisms of noise-resistance in genetic oscillators. Proc. Natl. Acad. Sci. U. S. A. 99 (9), 5988–5992.
Williams, S.B., et al., 2002. Structure and function from the circadian clock protein KaiA of *Synechococcus elongatus*: a potential clock input mechanism. Proc. Natl. Acad. Sci. U. S. A. 99 (24), 15357–15362.
Wolf, J., Becker-Weimann, S., Heinrich, R., 2005. Analysing the robustness of cellular rhythms. Syst. Biol. (Stevenage) 2 (1), 35–41.
Yoda, M.et al., 2007. Monomer-shuffling and allosteric transition in KaiC circadian oscillation. PLoS ONE 2 (5), e408.